Proceedings World Geothermal Congress 2020+1
Reykjavik, Iceland, April - October 2021

Geophysical and Geochemical Characterization of Menengai Geothermal System, Kenya

Isaack Kanda [1] and Yasuhiro Fujimitsu[2]

[1]Graduate School of Engineering, Department of Earth Resources Engineering, Faculty of Engineering, Kyushu University, Fukuoka 819-0395, Japan.

[2]Department of Earth Resources Engineering, Faculty of Engineering, Kyushu University, Fukuoka, 819-0395, Japan.

Keywords: magnetotelluric, gravity, Menengai geothermal field, 3-D inversion, isotope geochemistry

ABSTRACT

Menengai volcano is a late Quaternary caldera volcano formed on a massive shield in the inner-trough of the Kenya rift valley, associated with a high thermal gradient as a result of shallow magmatic intrusions. Menengai geothermal area lies within the central part of this rift section, which is characterized by an intricate geological set up associated with regional uplift referred to as the Kenya dome. In this study, the geothermal characteristics of the field were evaluated by using chemical and isotope data as well as 3-D inversions of both magnetotelluric (MT) and gravity data. The purpose was to image the subsurface geothermal structure with a view of confirming and delineating the extent of the geothermal resource. Integration of gravity data and resistivity data show a good relationship where regions with relatively low densities corresponded well with high resistivity zones. The high-density body of Olrongai (i.e., more than 2500 kg m−3) appears to mantle the resistive part (i.e., more than 90 Ω.m) while the resistive body inside Menengai caldera seems to surround a high-density structure. Anomalously high 3He/4He isotope from geothermal wells lies atop the dense body. The results reveal a possible pocket of a molten body that was emplaced as a dike at a shallow level, connected to a deeper magma chamber.

1. INTRODUCTION

The Menengai caldera and the Olrongai areas are manifested by signatures of high-temperature geothermal resource that include relatively young volcanism represented by numerous recent eruptions within and outside the caldera. The occurrence of active fumaroles (with temperatures between ~62 and ~88°C), steaming ground and warm water boreholes (e.g., Mungania & Lagat, 2004), implies that the area overlays an active hydrothermal system. The occurrence of such hydrothermal systems inside the caldera has already been confirmed by drilling (e.g., Omenda, Simiyu, & Muchemi, 2014).

The Bouguer anomaly reveals high-density values trending NNW-SSE with a dominant two-fold anomaly located to the north-northwest of the caldera and within the caldera. The low Bouguer anomalies are associated with Solai graben and Rongai plain located to the north-east and south-west areas, respectively. The high Bouguer anomalies appear to be confined within the caldera and the Olrongai area. This chapter gives a combined interpretation of the results obtained from this study focusing on the caldera and Olrongai areas.

2. GEOLOGY AND TECTONIC SETTING

The Menengai geothermal field is located in the central segment of the Kenya rift and is hosted partly within a major Quaternary volcano with Menengai caldera being central for its geothermal resource and conspicuously the major geological feature in the area (see Figure 1). This area is characterized by a complex geological setting associated with uplifted region the so-called Kenya dome, a geographical upwelling province of anomalously high elevations situated at the confluence of structures that resulted from major tectonic events and is covered for the most part by Cenozoic volcanic rocks (e.g., Corti, 2011; Davis & Slack, 2002; Leat, 1991; Savage & Long, 1985). This elliptical-shaped hoisted Kenya dome is a local culmination on the eastern rim of the East African plateau (e.g., Baker & Wohlenberg, 1971) conspicuously marked by three major central volcanoes; Mounts Kenya and Elgon in Kenya, and Mount Kilimanjaro in the Tanzania side.

The caldera volcanoes of the Kenyan rift are all to some extent unique, despite their close geographic proximities. Their variation is evidenced by their structural setting, the geological makeup, the interplay of their petrogenetic processes, and the mechanism of caldera collapse. All these factors encompass many of the features of peralkaline silicic systems globally (Ray Macdonald, 2012). At Menengai, two episodes of caldera formation of Krakatoan-type were accompanied by an eruption of a major ignimbrite and associated pumice and ash falls *(Leat, 1984)*.

The Menengai caldera is distinguished by the existence of a graben confined within a fault segment, and its partial collapse features suggest that portions of adjoining caldera wall also represent surface expressions of an embayed ring-fracture (see Figure 2). Such faults are not common in the Kenya rift valley, which is a tectonic province typically described by numerous parallel normal faults (e.g., Fairhead et al., 1972; Leat, 1984; McCall, 1967). Leat (1984) observed that the ring-fault architecture must have been controlled by a local crustal anomaly at Menengai and is well explained by causing collapse into a magma chamber, and the voluminous ash-flow tuff as a single flow unit suggests that the magma must have been stored, prior to eruption, in a vast, shallow reservoir.

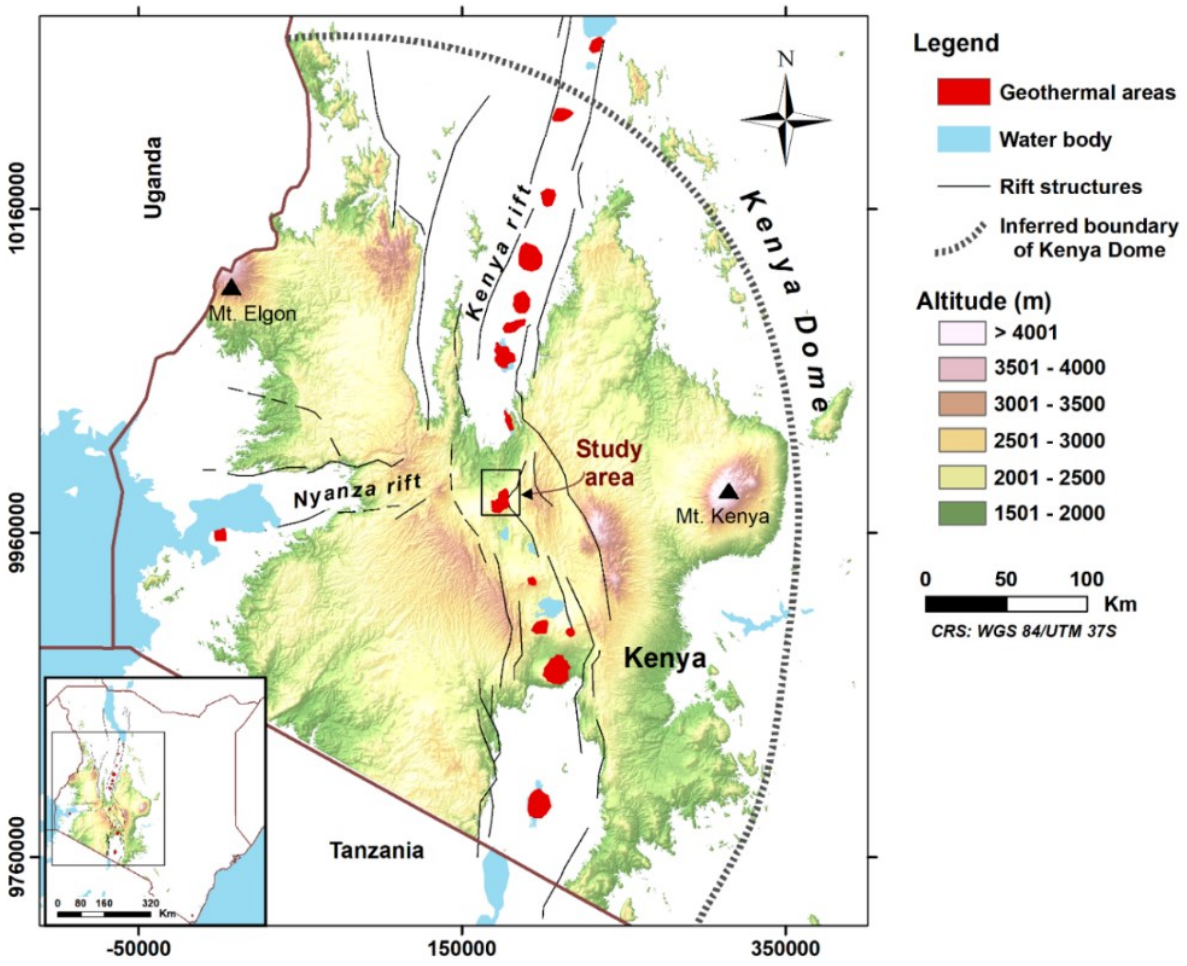

Figure 1: Location map of the study area. The high altitude (>1500 m above sea level) area shows part of the Kenya dome.

The occurrence of fumarolic activities is associated with the presence of fault structures that provide a means of access for hydrothermal fluids to reach the surface. In the same way, diffuse soil degassing study conducted shows that Carbon Dioxide (CO_2) and Radon 220 emanating from faults in Menengai were measured to be anomalously higher than background values, which was taken to insinuate existence of deep-seated crustal faults that tap and channel magmatic CO_2 to the surface where it is released through the soil (Kanda, 2010b).

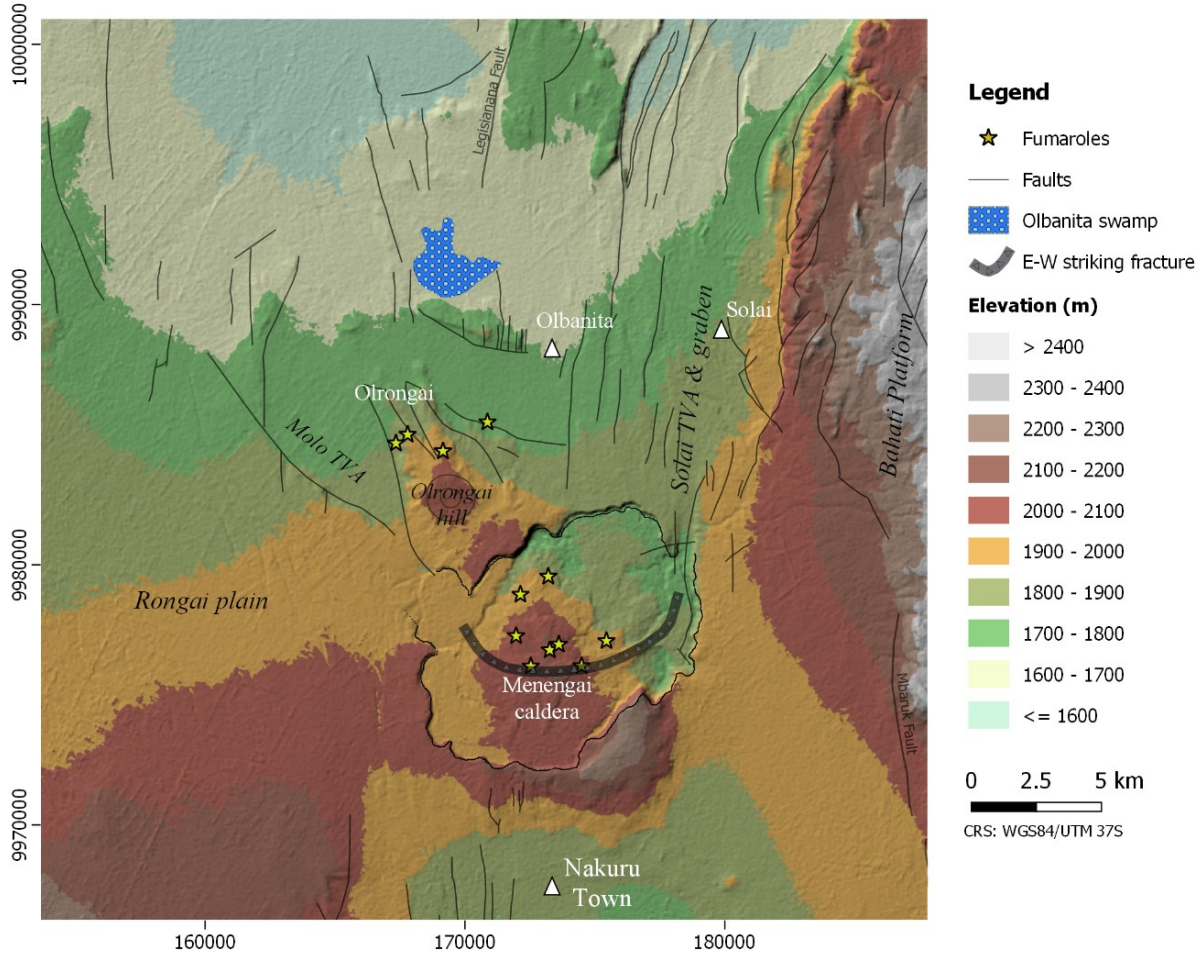

Figure 2: Descriptive map of the study area showing the elevation (m), faults, fracture and location of fumaroles.

The local surface geology is composed mainly of unconsolidated low-density volcanic soil and sediments, and tuffs & ignimbrites (Figure 3). The rest of the geology comprises of relatively higher density formations predominantly phonolites, trachytes, and basalts. Menengai Geothermal Prospect itself is located in an area characterized by an intricate tectonic activity linked with the rift triple junction. The triple junction is a zone at which the failed rift arm of the Nyanza rift joins the central Kenyan rift. Two rift floor volcano-tectonic axes that are important in controlling the geothermal system in the study area are the Molo and the Solai TVA. The main trend of the tectonic structures in the study area is the same as that of the rest of Kenyan Rift, which is mainly of N-S, NE-SW, and NW-SW, predominantly lying to the north of the caldera (see Figure 3).

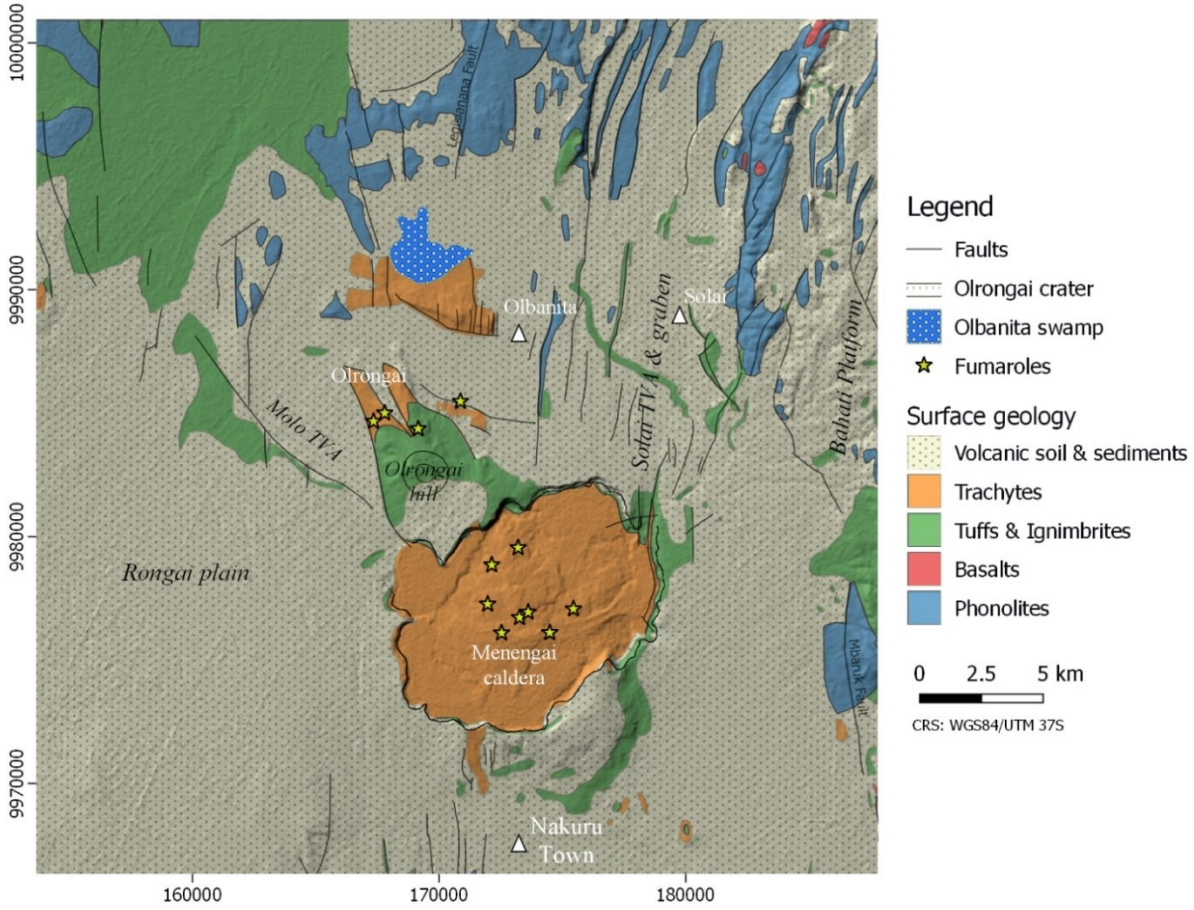

Figure 3: Surface geology map of the study area, modified from previous work done by *McCall (1967)*, *Jennings (1971)* and *Walsh (1969)*.

The nature of post-caldera emplacement of trachytic formation and ash-flow tuffs is quite complex and is related to many eruptions. The products of these eruptions cover the caldera floors and make it difficult to delineate important geological structures essential for geothermal exploitation without the help of geophysical methods. The Menengai caldera is formed on a large exposed joint at the tailcrack culmination of the northerly striking dextral normal oblique slip-fault region (Chorowicz, 2005), which seems to be connected with a series of NNE trending normal faults. These faults cut across the caldera wall, and they perhaps contributed to the existence of the caldera.

This large open crack curls across the caldera from east to west and appears to have acted as a conduit of eruptives to the surface as supported by an underlying dense body. The faults consequentially render the caldera wall incomplete as they cut through the northeastern rim by north-south trending segment graben (McCall, 1967), marking the southern end of Solai graben. This graben runs along a swarm of very young faults that cut the rift valley floor from Menengai northwards. Kinematic assessment inside the caldera relates these faults with strike-slip and oblique-slip transfer faults, commonly seen across the central Kenyan rift (Riedl, Melnick, Mibei, Njue, & Strecker, 2015). The activation of these regional faults allowed trachytic magma to ascend to shallower levels, which then flows laterally being accommodated by permeable fault zones.

3. METHOD AND DATA PROCESSING

A total of 630 gravity stations, 212 MT soundings and $^{3}He/^{4}He$ ratio data of 15 wells were used in this study. The gravity dataset consists of those acquired in 2016-2017, combined with previous data by Mungania & Lagat (2004), Geotermica Italiana (1987) and Bureau Gravimétrique International – BGI (Drewes, Kuglitsch, Adám, & Rózsa, 2016). MT data used were collected by Lagat et al. (2010). The 3-D inversion of the Bouguer gravity anomaly was carried out using VOXI 3D Inversion, built within the Oasis Montaj platform. The MT data were inverted in the period range of 10^{-3} –10^{3} s to image the 3-D resistivity structure of using ModEM inversion code (Egbert & Kelbert, 2012).

4. RESULTS AND DISCUSSION

4.1 Menengai Caldera

The idea of interpreting the two geophysical methods together was to give a better understanding of the structures controlling the geothermal system in the study area. The two methods were based on density and resistivity distribution below the earth

surface. To achieve this, the resistivity profiles were chosen to intersect the high-density body in order to support the obtained results hence to give more insights into major subsurface structures governing the geothermal system (Figure 4). Since the two resistivity profiles intersect each other, they appear to image the same geophysical structures.

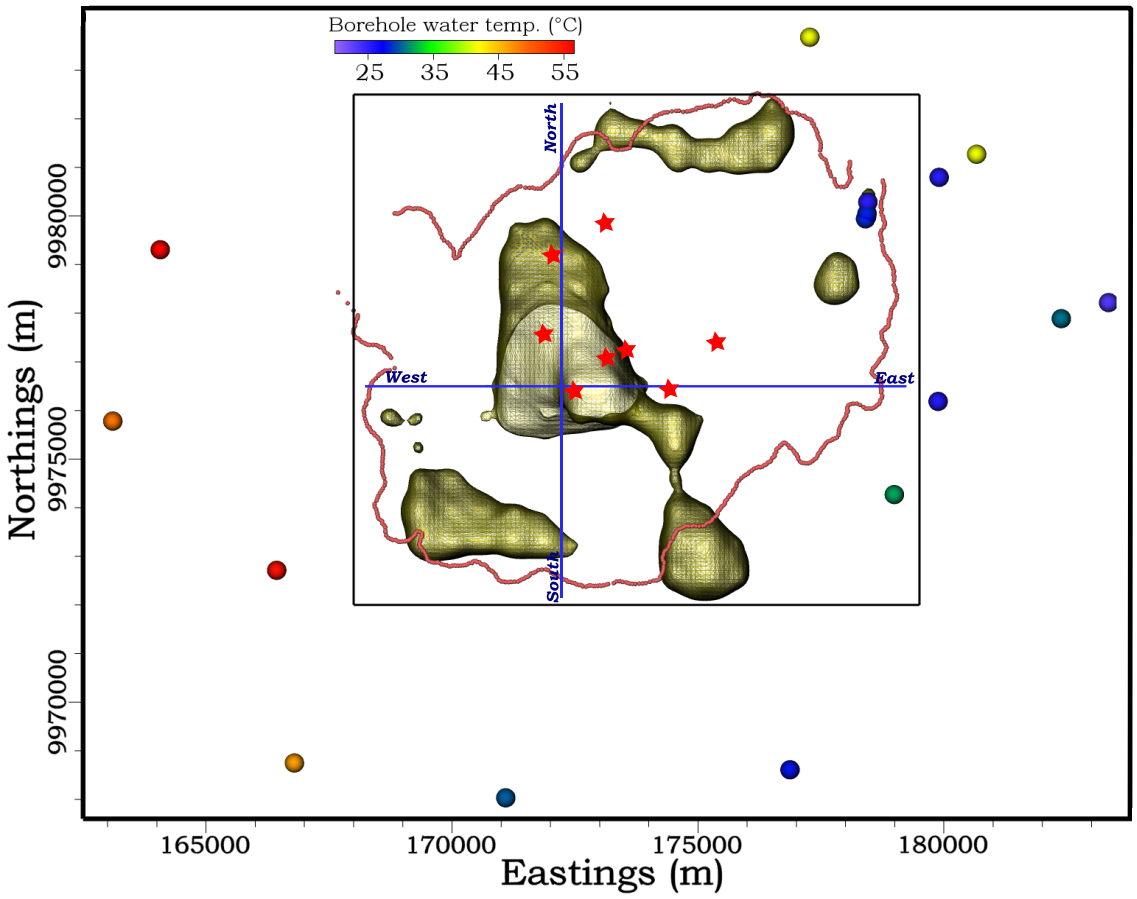

Figure 4: Menengai caldera map showing the location of the 3-D MT inversion profiles (blue line) along West-East and South-North directions. The cross-sections are shown in Figure 5 and Figure 6. A density isosurface of 2.55×10^3 kg m^{-3} extracted from 3-D gravity model is also plotted. Temperature (ranging from 20 – 57 °C) of water drawn from boreholes spread around the study area is indicated by colored dots. The fumaroles are presented as red stars.

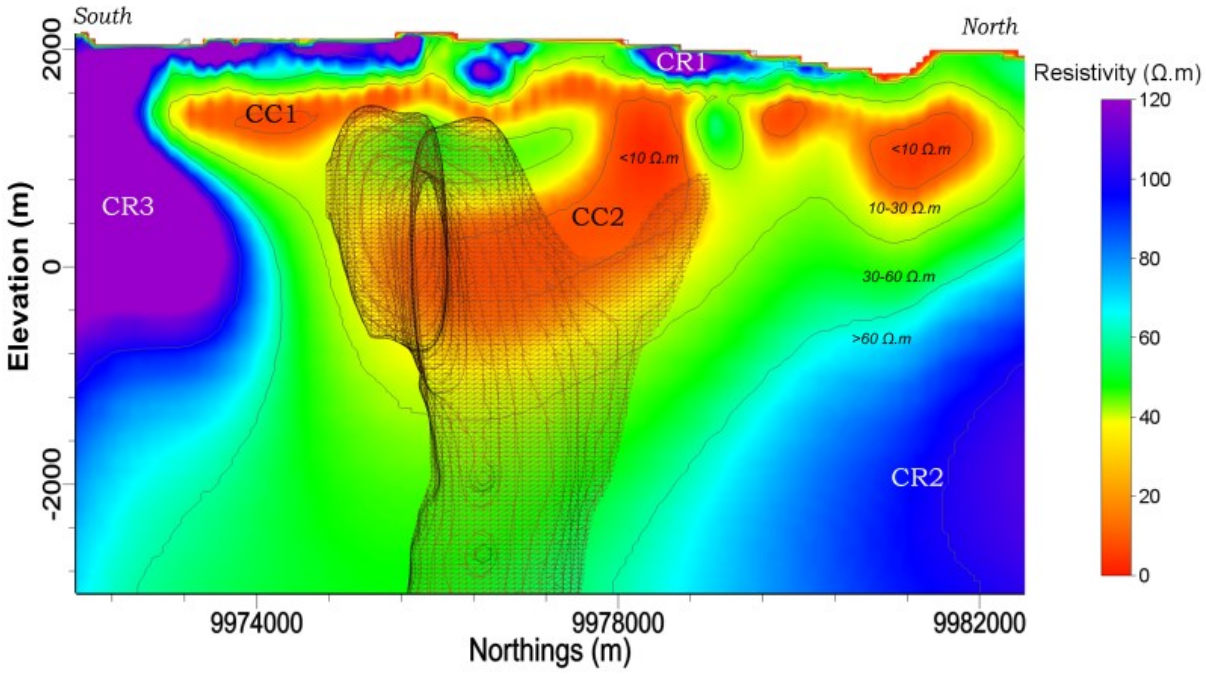

Figure 5: South-North cross-section of 3-D resistivity model and a density isosurface of 2.55 × 10^3 kg m^{-3} (shown as a mesh) extracted from the 3-D gravity model.

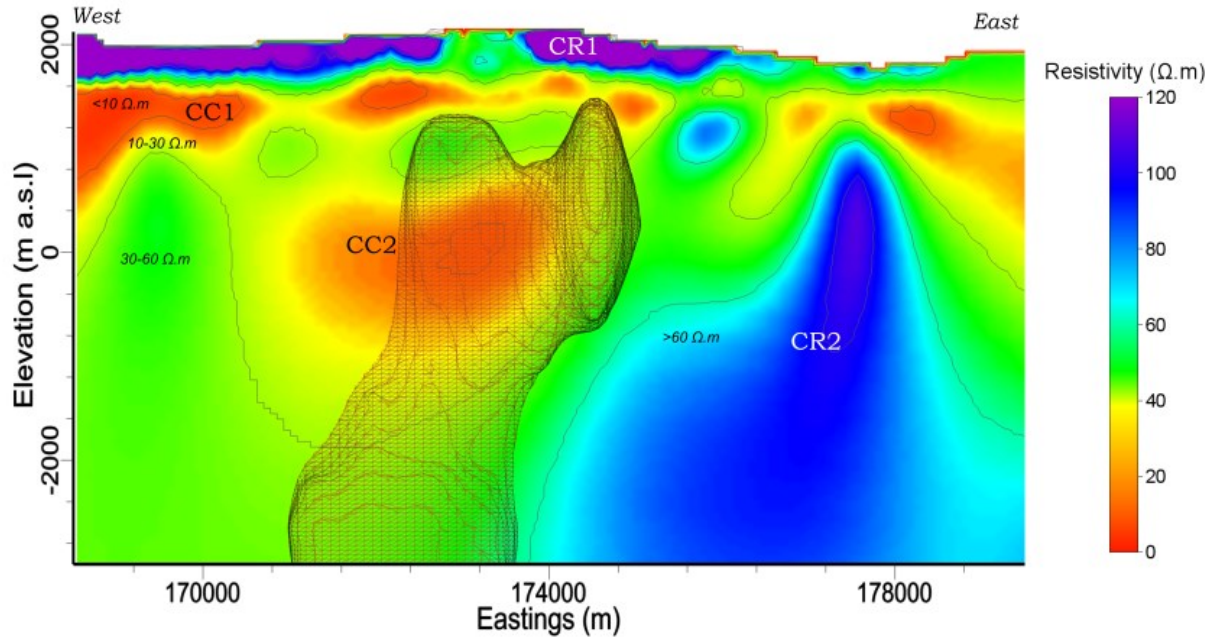

Figure 6: West-East cross-section of the 3-D resistivity model and a density isosurface of 2.55 × 10^3 kg m^{-3} (shown as a mesh) extracted from the 3-D gravity model.

Figure 5 shows the south-north resistivity section that was obtained from the 3-D MT inversion and density isosurface of 2.55 × 10^3 kg m^{-3} taken from the 3-D gravity model. The conspicuous highly resistive body (CR3) to the south coincides with the caldera wall while the other resistive body (CR2) is observed on the northern part of the caldera, which can be interpreted as a cold formation. The other obvious feature is the conductive layer (CC1) which appears to connect a relatively deeper

conductor (CC2). This CC2 appears to lie on top of the dense body from the gravity model suggesting a close relationship between the bodies.

The cross-section in Figure 6 is aligned in a west-east direction and displays noticeable resistivity structures. One of these structures is a resistive layer (CR1, > 120 Ω.m) that can be interpreted as unaltered formation near the ground surface, which spreads across, particularly to the west of the caldera floor. A deeply seated resistive body (CR2, > 100 Ω.m) is found on the eastern part which perhaps can be regarded as a cold formation. Conductors CC1 and CC2 are imaged the same way as in Figure 5.
The high resistive body CR2 in Figure 7 appears to surround the high-density anomaly, and this suggests the occurrences of the two geophysical structures are interrelated. This dense structure is located within the conductive zone, away from the resistive structure and this might be caused by the deep circulation of chemically altered hydrothermal fluid. Such deep fluid movement is likely to occur with the help of geological structures that can allow free fluid motion, and this can be corroborated by the occurrence of fumarolic activities confined within this region. However, the dense structure and the resistive body (CR3) appear to coexist on the southern segment of the caldera wall that forms the remaining part of the Menengai shield volcano (Leat, 1991).

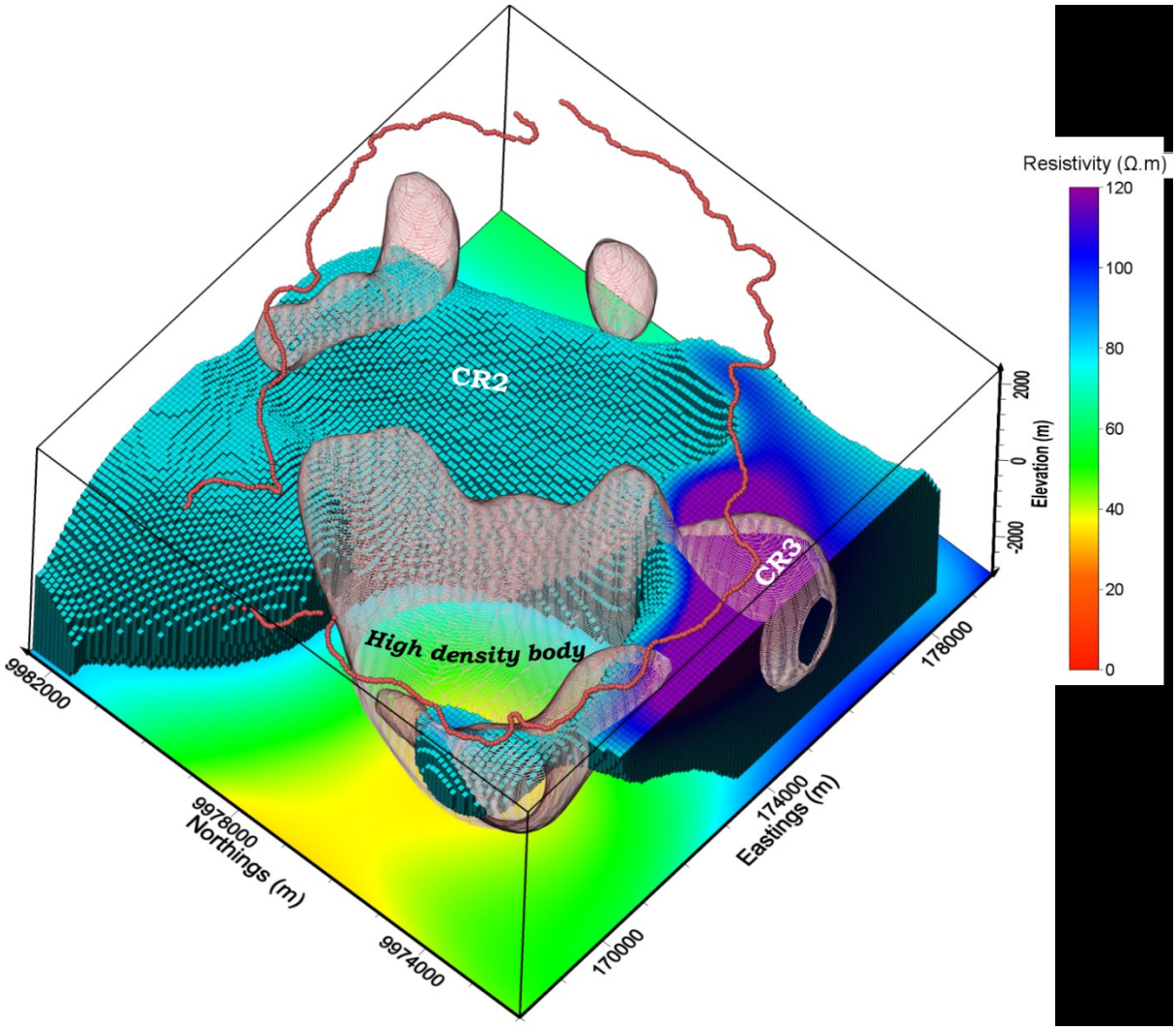

Figure 7: 3-D perspective view of the resistive isosurface (blue blocks (CR2), >90 Ω.m) and 3D geometry of the dense body isosurface (transparent mesh, >2.55 × 10^3 kg m^{-3}) of caldera area. The planar view is a horizontal slice of density anomaly at 3000 m bsl.

Figure 8 presents a perspective view of 3-D gravity and resistivity models of the caldera. The main features identified include the near-surface conductor overlaying the dense body and stretching to the west interpreted as the upflow and outflow zones, respectively. In Figure 4, the distribution of boreholes with measured water temperature ranging from 20-57 °C is presented. Those groundwater boreholes with higher temperatures are located to the west and south-west of the caldera and perhaps fed by thermal fluid outflowing from the Menengai geothermal system. The outflow might then be responsible for the formation of the alteration zone to the west of the caldera as shown in Figure 6 and Figure 8.

The deeper conductive zone positioned together with the dense body is likely to be the heat source. Most of the production wells are located above or close to this deeper conductor, and the hottest wells have intercepted temperatures close to 400 °C (GDC, 2018). The proposed recharge zone lies within the resistive region which might be caused by cold water incursion. The location of this zone also is in line with the assumption that the general flow of fluid from this region is northwards as supported by piezometric and structural studies (Mungania & Lagat, 2004).

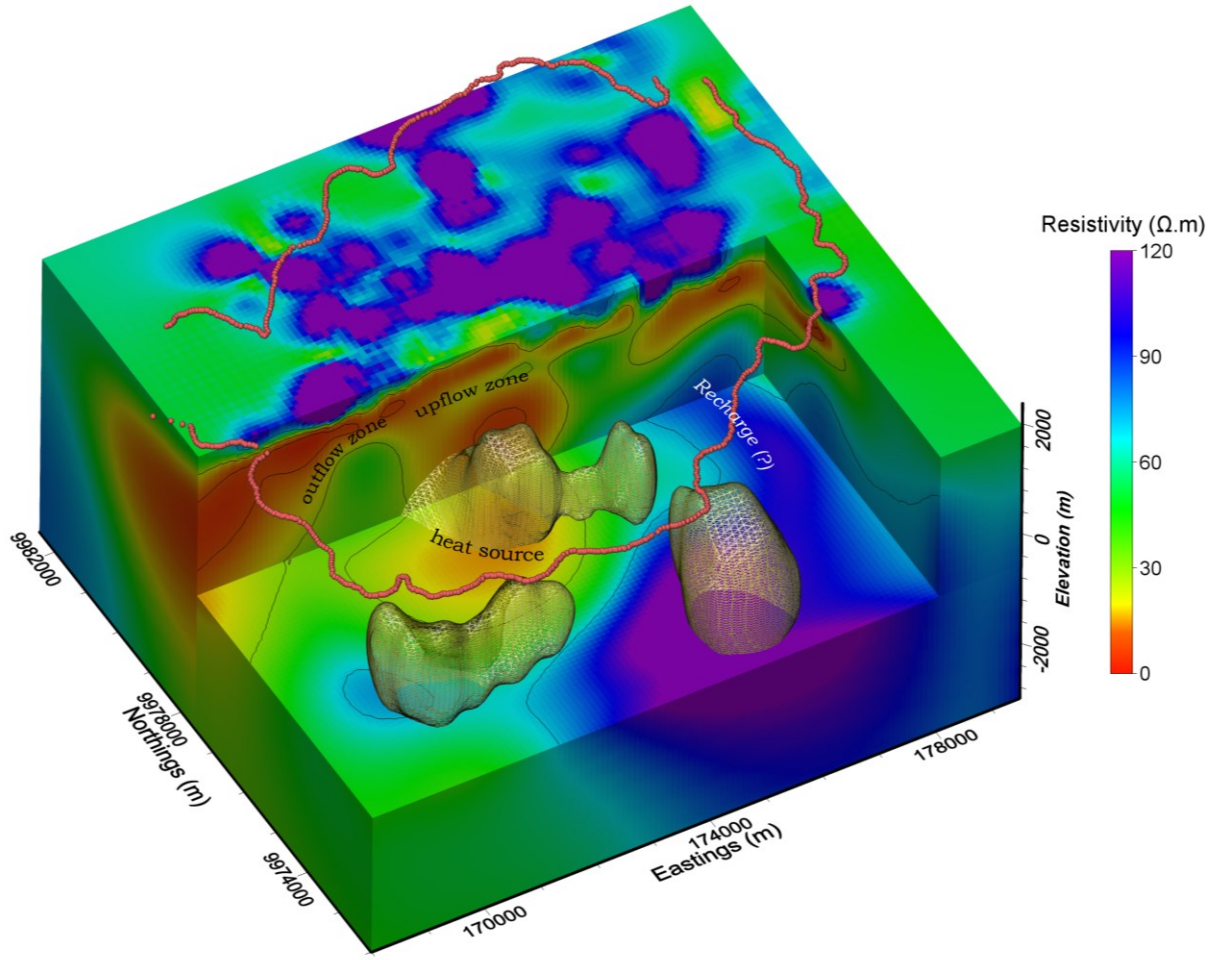

Figure 8: A perspective model of the 3-D gravity and magnetotelluric inversions of the Menengai caldera area. The block represents magnetotelluric results whereas the transparent mesh indicates the dense body isosurface (2.55×10^3 kg m^{-3}).

Figure 9 shows that the high $^3He/^4He$ coincides with the highly conductive body beneath Menengai caldera. The anomalous $^3He/^4He$ isotopes and the conductive layer appear to sit on top of the dense body. This implies that the highly conductive zone is a cooling body of magma or a partial melt that was emplaced as a dike and is connected to a deeper magma chamber. The magma chamber taps from the mantle and hence the high $^3He/^4He$ anomaly appears.

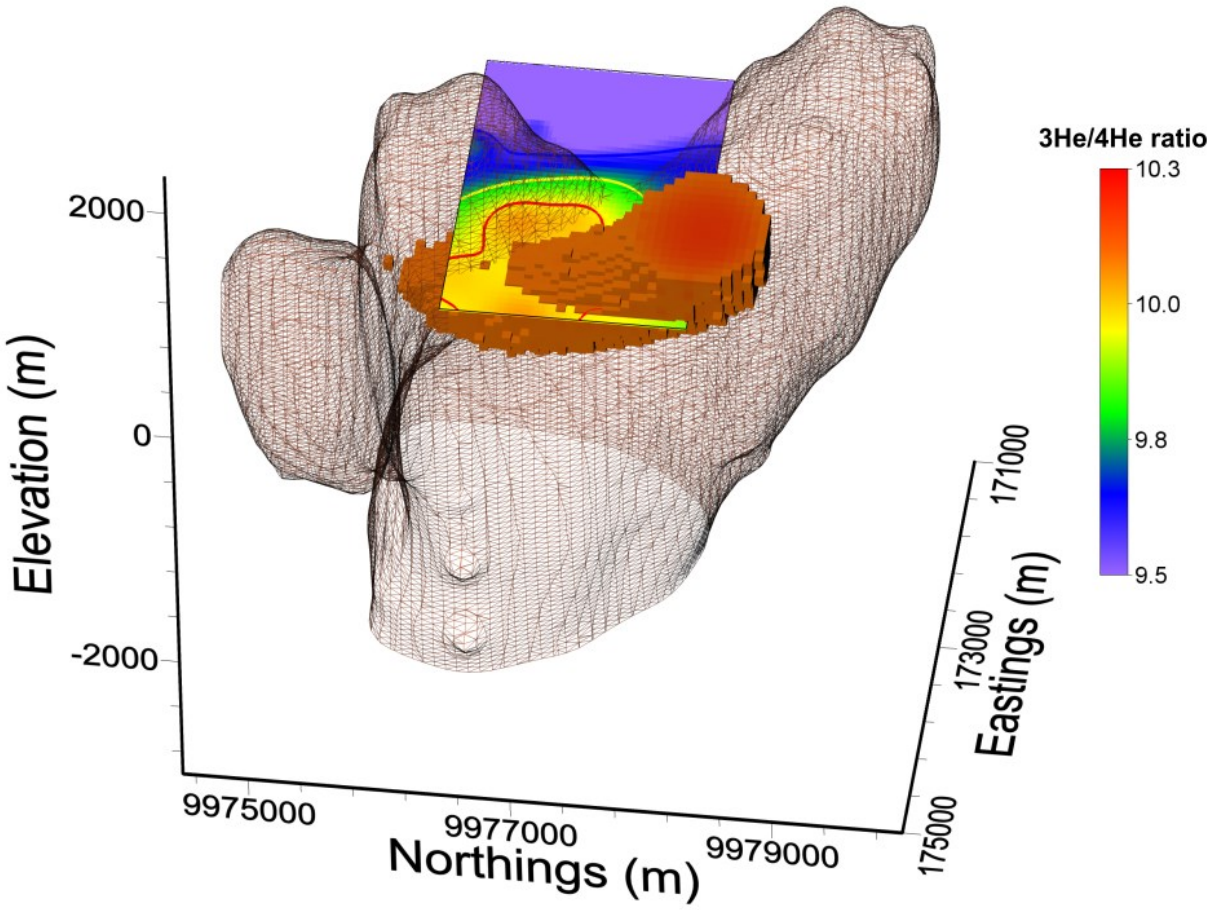

Figure 9: A joint model 3-D gravity and magnetotelluric inversions, and $^{3}He/^{4}He$ isotopes contour map (referenced at an elevation of -500 m a.s.l) of the Menengai caldera area. The block represents magnetotelluric result (<10 Ω.m) whereas the transparent mesh indicates the dense body isosurface (2.55×10^{3} kg m^{-3}).

4.2 The Olrongai Area

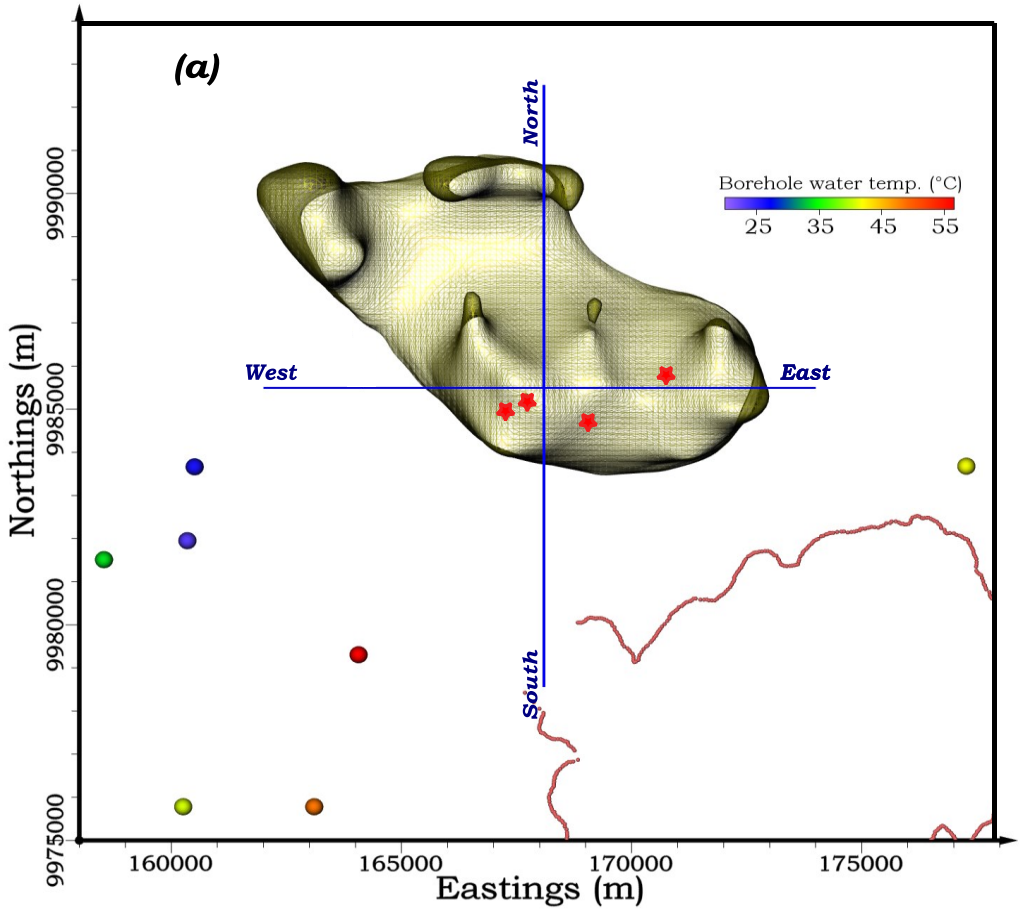
(a)
North
West
East
South
Borehole water temp. (°C)
25 35 45 55
Northings (m)
9990000
9985000
9980000
9975000
160000
165000
170000
175000
Eastings (m)

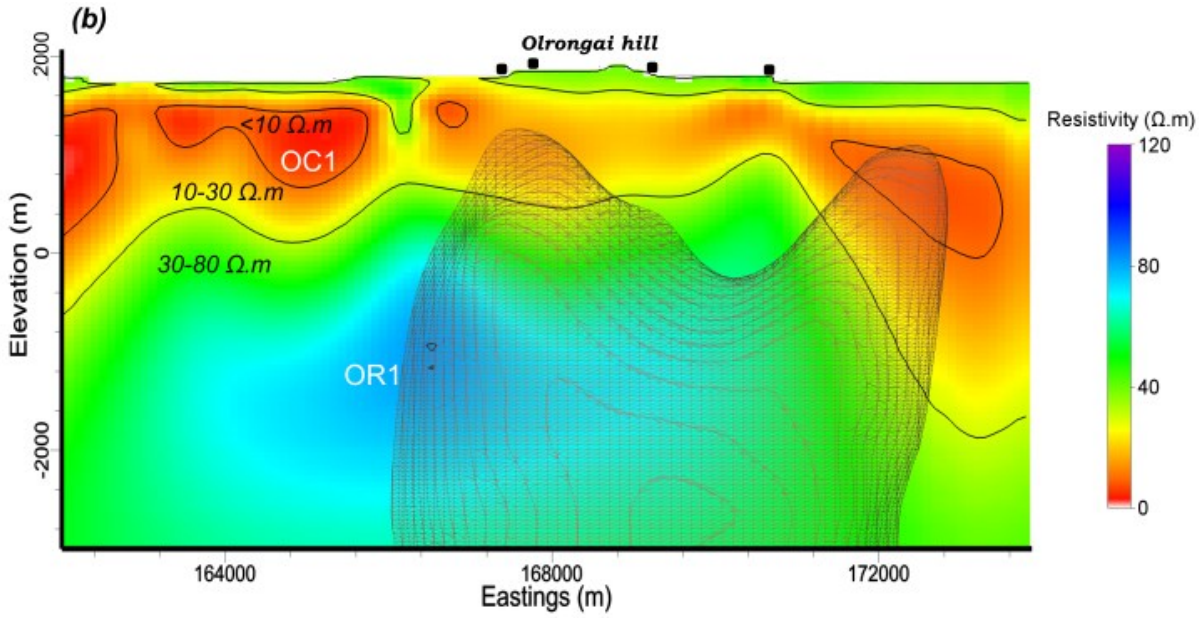
(b)
Olrongai hill
<10 Ω.m
OC1
10-30 Ω.m
30-80 Ω.m
OR1
Elevation (m)
2000
0
-2000
164000
168000
172000
Eastings (m)
Resistivity (Ω.m)
120
80
40
0

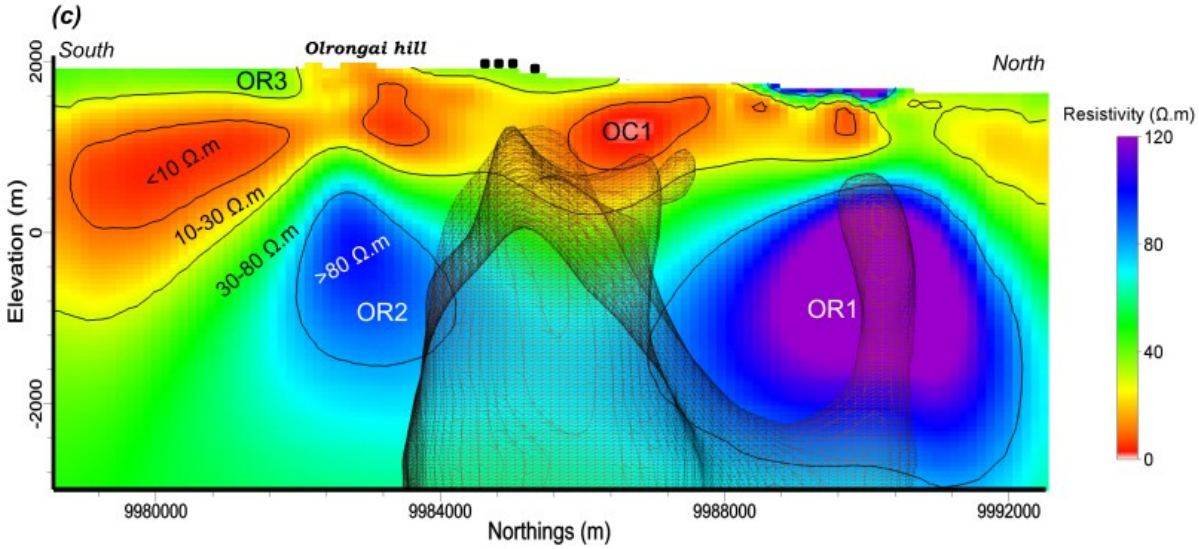

Figure 10: Cross-sections of 3-D resistivity model (b and c) along profiles 'west-east' and 'south-north' indicated on (a) in the Olrongai area. On each of the cross-section, a density isosurface of 2.5 × 10^3 kg m^{-3} extracted from the 3-D gravity model is also plotted (also plotted on (a)). Circles in Figure 10 a show temperature (ranging from 20 – 57 °C) of water drawn from boreholes spread around the study area. The orange line, the red stars (shown as black squares in b and c) and brown lines in Figure 10 are the Menengai caldera rim, fumarole locations, and geological faults, respectively.

Figure 10b-c show the west-east and south-north resistivity cross-section extracted from the inversion model and density isosurface of 2.5 × 10^3 kg m^{-3} extracted from the density model. The resistivity sections describe the main features of the Olrongai subsurface structures. Generally, the shallow depths are characterized by a resistive layer (OR3) of more than 60 Ω.m followed by pockets of conductive zones (OC1) with a resistivity value below 10 Ω.m sandwiched within transitional areas, whose resistivity range from 10 – 30 Ω.m. Beneath this layer is a region with resistive values greater than 30 Ω.m (OR1). In this region, resistivity increases gradually up to >120 Ω.m away from the dense body, and particularly to the north of the dense body as shown in Figure 10c. The upper boundary of OR1 zone (> 30 Ω.m) varies across the study area and ranges between elevations of 2000 m a.s.l (right above OR1) and sea level in the east and west (Figure 10b), and south (c) directions.

The low resistivities observed in the near-surface section is caused inferably by hydrothermal alteration of the young rocks of Athinai Trachyte (and probably also Olrongai Ignimbrites) formations, due to a higher temperature and acidic fluid emanating from the magma body. The resistivity of this layer, commonly known as the smectite zone (mainly in the range of 1-10 Ω.m), is usually determined by the type and intensity of alteration process, transformed by the amount of water saturation and temperature (e.g., Anderson, Crosby, & Ussher, 2000; Ussher, Harvey, Johnstone, Anderson, & Zealand, 2000). At depths greater than ~1000 m, the resistivity values increase most probably due to changes in the clay-type ensuing from hydrothermal alteration process. The alteration products at higher temperatures are less conductive and are typically illitic and chloritic clays replacing the smectite, the latter is unstable at higher temperatures. Therefore, the hotter part of the geothermal system beneath the highly conductive clay cap, interpreted as the heart of the reservoir, is characterized by relatively higher resistivities. However, away from the active part of the system, resistivity decreases as the depth increases. The relatively low resistive region to the left of the dense body (see Figure 10c) can be interpreted as the recharge zone for the geothermal system.

Figure 10a shows distributions of boreholes with measured water temperature ranging from 20 – 57 °C. Those with higher temperatures are located in the southern part of the area and beyond. Based on the resistivity results of a south-north cross-section of the area shown in Figure 10c and the north-south trending structures, these boreholes appear to be tapping from the outflow zone of the Olrongai geothermal system.

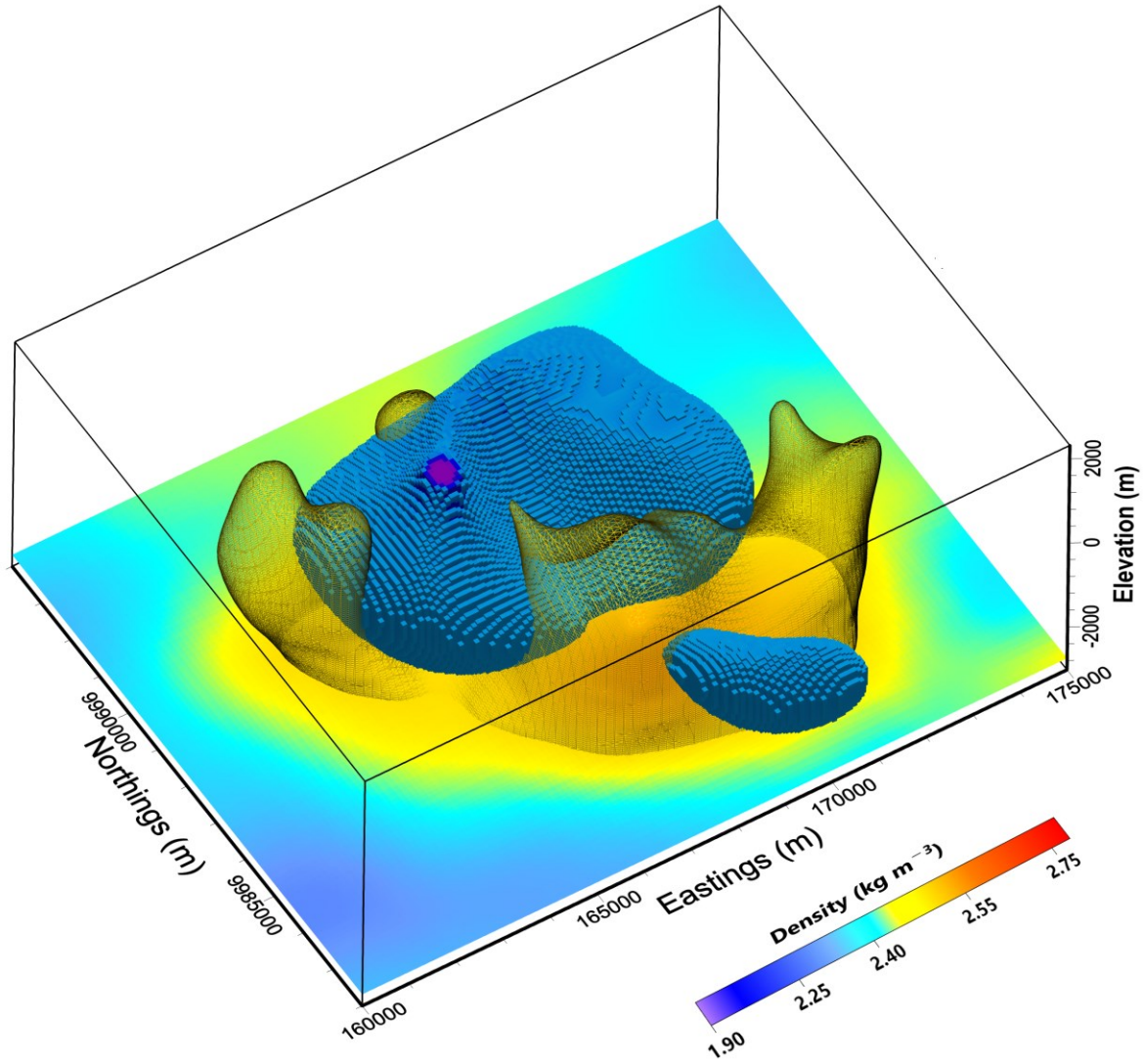

Figure 11: 3-D perspective view of the resistive isosurface (blue blocks, >90 Ω.m) and 3D geometry of the dense body isosurface (transparent mesh, >2.5 × 10^3 kg m^{-3}) of Olrongai area. The planar view is a horizontal slice of density anomaly 3000 m bsl.

One of the most attractive features of the gravity and MT inversion models is the relationship in the geometry of the dense body relative to the resistive body. Figure 11 displays the 3-D view of the high resistive isosurface (>90 Ω.m) and the high density (>2.5 × 10^3 kg m^{-3}) bodies from the inversion models. The dense body appears to mantle the resistive part showing that the two have different formation properties. There is evidence of volcanic fluids rising beneath the summit of the dense body as interpreted by the presence of fumarolic activities and low resistivity in the region. This decrease in resistivity may have resulted from the effect of acidic waters formed by the interaction of local groundwater with rising steam and gases of volcanic origin causing intense hydrothermal alteration of the volcanic rocks at the upflow zone and fades laterally away at the outflow. However, there is no indication that the volcanic-hydrothermal system extends laterally much to the north of the study area. Figure 12 shows a clay layer that deepens away from the dense body and suggesting that the fluid flow away from this central part. The proposed recharge zone is based on the assumption that the general flow of fluid from this region is northwards as supported by piezometric and structural studies (Mungania & Lagat, 2004).

Mungania & Lagat (2004) carried out fumarole flow rates, and heat loss measurements in this area from a shallow temperature gradient. The temperatures were obtained on the surface and at the depths of 25 cm, 50 cm, and 100 cm in the holes they drilled. The natural heat flow results showed that areas with intense thermal activity near the summit of Olrongai hill coincided with the locations of fumaroles. Beneath this thermally anomalous region is the heart of the dense body and extends in east and west directions, which can be interpreted as the Athinai Trachytes (Leat, 1991; R. Macdonald, Baginski, Leat, White, & Dzierzanowski, 2011).

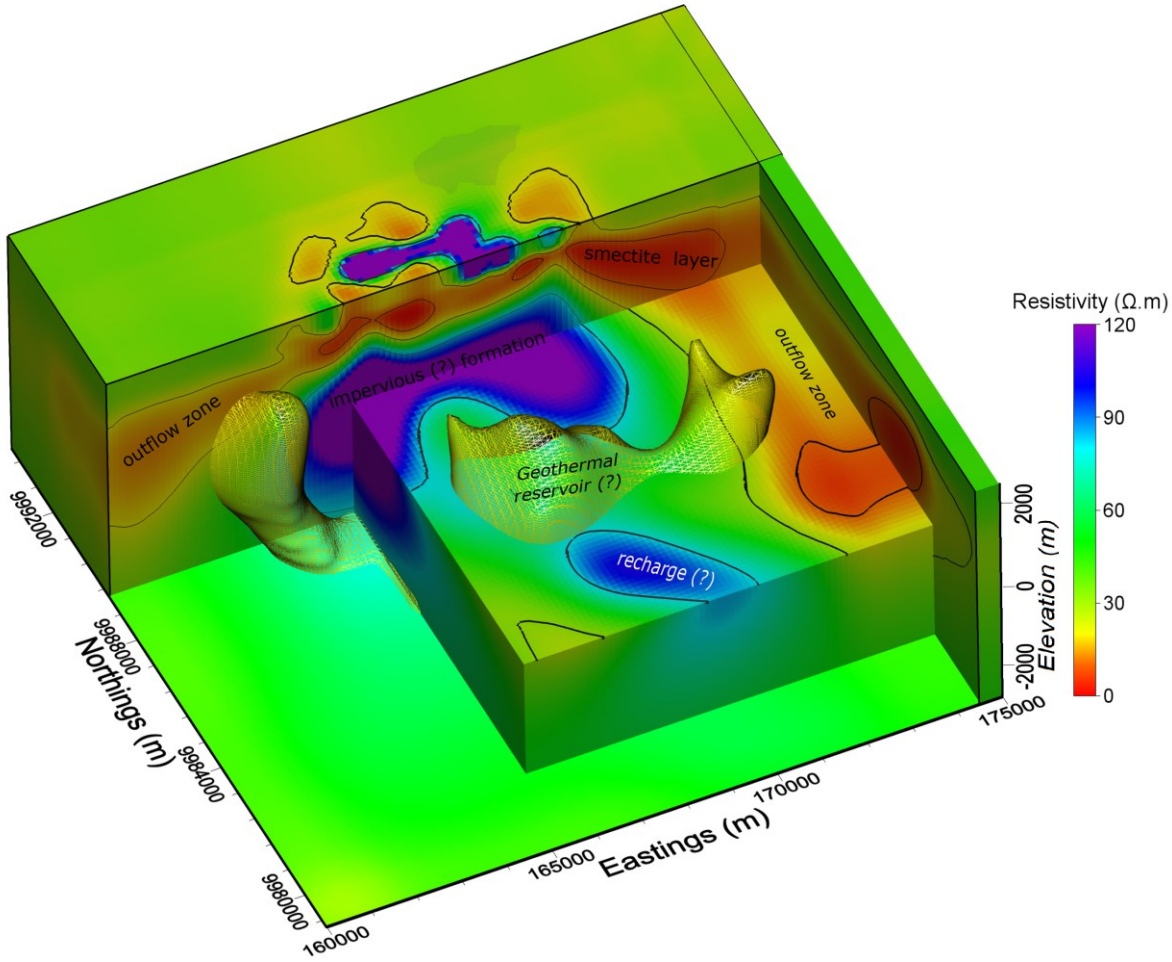

Figure 12: A perspective model of 3D gravity and magnetotelluric inversions in the Olrongai area. The block model represents magnetotelluric results whereas the transparent mesh indicates the dense body isosurface (2.5×10^3 kg m^{-3}).

The Olrongai area is dominated by dry, perched-aquifer and thermally anomalous boreholes, where the productive ones are very shallow with low-yield (< 6 m^3/hr) that get depleted fast since the deeper formations are impervious (Mungania & Lagat, 2004). The aquifers of the low-yield boreholes are located at the contacts between tuff and ignimbrite beds. The perched ones are adjacent to the Olbanita swamp (Figures 2 & 3), which lies right above the northern end of the highly resistive body (Figure 12). This swamp is fed by a seasonal river and owes its existence to impervious ignimbrite beds that have been affected by hydrothermal alteration. The ignimbrite is densely welded, with rheomorphic flow structures and consists of trachytic pumices and lithic clasts mostly trachyte or trachyphonolite lava (Leat, 1991). Ignimbrite usually is characterized by low density (1.21–1.93 $\times$ 10^3 kg m^{-3}) and high porosity (18–51%) (e.g., Moon, 1993) and from the model we infer that the high resistive and relatively low-density body beneath the Olrongai area is predominantly composed of an impervious Olrongai Ignimbrite formation with a conservative computed volume of ~63 km^3. Nonetheless, Leat (1991) reported the presence of much younger air-fall pumice and tuffs that were emplaced alongside Athinai Trachytes. Alternatively, this resistive body could as well be interpreted as cold formation. In this case, the water from the swamp Olbanita might have seeped down through the existing faults possibly recharging the geothermal system.

5. CONCLUSION

This study presents the integrated interpretation of geochemical and geophysical methods used to characterize the subsurface structures of the Menengai geothermal area. From the inversion results of gravity and MT data, the relationship in the geometry of the dense body could be identified relative to the resistive body. The high-density body (> 2.5 $\times$ 10^3 kg m^{-3}) appear to mantle the high resistive part (> 90 Ω.m) showing that the two structures have different formation properties. This relationship shows that the two geophysical structures have different properties. The resistive body is interpreted as cold or relatively impervious structures. A cold formation/structure would suggest a possible recharge to the geothermal reservoir.

The presence of fumarolic activities and low resistivity in the region is attributed to the rise of volcanic fluids beneath the summit of the dense body where the heat source is believed to be hosted. This decrease in resistivity may have resulted from the effect of acidic waters formed by the interaction of local groundwater with rising steam and gases of volcanic origin causing intense hydrothermal alteration of the volcanic rocks at the upflow zone and fades laterally away at the outflow. The gases appear to emanate from the mantle as confirmed by the presence of anomalously high $^{3}He/^{4}He$ from well discharge chemistry. The anomalous $^{3}He/^{4}He$ isotopes from the geothermal wells located on top of the dense body imply that the highly conductive zone is likely to be a cooling body of magma or a partial melt emplaced as a dike and is connected to a deeper magma chamber.

REFERENCES

Anderson, E., Crosby, D., & Ussher, G. (2000). Bull's Eye! - Simple resistivity imaging to reliably locate the geothermal reservoir. In *Proceedings of the 2000 World Geothermal Congress* (pp. 909–914). Retrieved from https://www.scopus.com/record/display.uri?eid=2-s2.0-0242519110&origin=inward&txGid=84fada05d92c744c4806534084732363

Baker, B. H., & Wohlenberg, J. (1971). Structure and evolution of the Kenya Rift Valley. *Nature*, *229*(5286), 538–542. https://doi.org/10.1038/229538a0

Chorowicz, J. (2005). The East African rift system. *Journal of African Earth Sciences*, *43*(1–3), 379–410. https://doi.org/10.1016/J.JAFREARSCI.2005.07.019

Corti, G. (2011). Evolution and characteristics of continental rifting: Analogue modelinginspired view and comparison with examples from the East African Rift System. *Tectonophysics*, *in press*. https://doi.org/10.1016/j.tecto.2011.06.010

Davis, P. M., & Slack, P. D. (2002). The uppermost mantle beneath the Kenya dome and relation to melting, rifting and uplift in East Africa. *Geophysical Research Letters*, *29*(7), 1117. https://doi.org/10.1029/2001GL013676

Drewes, H., Kuglitsch, F., Adám, J., & Rózsa, S. (2016). The International Gravimetric Bureau. In "The Geodesist's Handbook 2016". *Journal of Geodesy*, *90*(10), 907–1205. https://doi.org/10.1007/s00190-016-0948-z

Egbert, G. D., & Kelbert, A. (2012). Computational recipes for electromagnetic inverse problems. *Geophysical Journal International*, *189*(1), 251–267. https://doi.org/10.1111/j.1365-246X.2011.05347.x

Fairhead, J. D., Mitchell, J. G., & Williams, L. A. J. (1972). New K/Ar Determinations on Rift Volcanics of S. Kenya and their Bearing on Age of Rift Faulting. *Nature Physical Science*, *238*(83), 66–69. https://doi.org/10.1038/physci238066a0

GDC. (2018). *Steam status and resource assessment of Menengai geothermal project, Kenya. Internal report*.

Geotermica Italiana. (1987). *Geothermal Reconnaissance Survey in the Menengai Bogoria area of the Kenya Rift Valley*.

Jennings, D. J. (1971). *Geology of the Molo Area* (No. 86).

Kanda, I. (2010). Structural controls on thermal anomalies and diffuse soil degassing at Menengai geothermal prospect, the Kenyan rift valley. In *Third African Rift Geothermal Conference* (pp. 67–72). ARGEO - C3.

Lagat, J., Mbia, P., Muturia, C., Njue, L., Kanda, I., Mutonga, M., … Mutia, T. (2010). *Menengai geothermal prospect: a geothermal resource assessment project report update*. Nakuru, Kenya.

Leat, P. T. (1984). Geological evolution of the trachytic caldera volcano Menengai, Kenya Rift Valley. *Journal of the Geological Society*, *141*(6), 1057–1069. https://doi.org/10.1144/gsjgs.141.6.1057

Leat, P. T. (1991). Volcanological development of the Nakuru area of the Kenya rift valley. *Journal of African Earth Sciences*, *13*(3–4), 483–498. https://doi.org/10.1016/0899-5362(91)90111-B

Macdonald, R., Baginski, B., Leat, P. T., White, J. C., & Dzierzanowski, P. (2011). Mineral stability in peralkaline silicic rocks: Information from trachytes of the Menengai volcano, Kenya. *Lithos*, *125*(1–2), 553–568. https://doi.org/10.1016/j.lithos.2011.03.011

Macdonald, Ray. (2012). Evolution of peralkaline silicic complexes: Lessons from the extrusive rocks. *Lithos*, *152*, 11–22. https://doi.org/10.1016/j.lithos.2012.01.014

McCall, G. J. H. (1967). *Geology of the Nakuru-Thomson's Falls-Lake Hannington Area: Degree Sheet No. 35 SW Quarter and 43 NW Quarter* (No. 78). *Geological Survey of the Kenya Republic* (Vol. 78). Geological Survey of Kenya.

Moon, V. G. (1993). Geotechnical characteristics of ignimbrite: A soft pyroclastic rock type. *Engineering Geology*, *35*(1–2), 33–48. https://doi.org/10.1016/0013-7952(93)90068-N

Mungania, J., & Lagat, J. (2004). *Menengai volcano: Investigations for its geothermal potential*.

Omenda, P., Simiyu, S., & Muchemi, G. (2014). Geothermal Country Update Report for Kenya: 2014. *001374011*, 29–31.

Riedl, S., Melnick, D., Mibei, G. K., Njue, L., & Strecker, M. R. (2015). Post-caldera faulting of the Late Quaternary Menengai caldera, Central Kenya Rift (0.20°S, 36.07°E). *EGU General Assembly 2015, Held 12-17 April, 2015 in Vienna, Austria.*, *17*.

Savage, J. E. G., & Long, R. E. (1985). Lithospheric structure beneath the Kenya Dome. *Geophysical Journal of the Royal Astronomical Society*, *82*(3), 461–477. https://doi.org/10.1111/j.1365-246X.1985.tb05146.x

Ussher, G., Harvey, C., Johnstone, R., Anderson, E., & Zealand, N. (2000). Understanding the resistivities observed in geothermal systems. *Proceedings World Geothermal Congress*, (May 2000), 1915–1920.

Walsh, J. (1969). *Geology of the Eldama Ravine-Kabarnet Area: Degree Sheet 34 SE Quarter*. *Geological Survey of the Kenya*. Nairobi.